Inorganic Chemistry
Article

Inorg. Chem. **2010**, *49*, 541–551 **541**
DOI: 10.1021/ic901614p

Copper(II) and Nickel(II) Complexes of β-Aminoketoxime Ligand: Syntheses, Crystal Structures, Magnetism, and Nickel(II) Templated Coupling of Oxime with Nitrile

Oindrila Das,[†] N. N. Adarsh,[‡] Ankan Paul,*[,§] and Tapan Kanti Paine*[,†]

[†]*Department of Inorganic Chemistry,* [‡]*Department of Organic Chemistry, and* [§]*Raman Center for Atomic, Molecular and Optical Sciences, Indian Association for the Cultivation of Science* (*IACS*), *2A & 2B Raja S. C. Mullick Road, Jadavpur, Kolkata 700032, India*

Received August 12, 2009

The syntheses, molecular structures, and magnetic properties of a dicopper(II) complex, $[Cu_2(HL^1)_2](ClO_4)_2$ (**1**), and its nickel(II) analog, $[Ni_2(HL^1)_2](ClO_4)_2$ (**2**), of a β-amino ketoxime ligand (H_2L^1 = 4,4,9,9-tetramethyl-5,8-diazadodecane-2,11-dione dioxime) are discussed. The metal centers in out-of-plane oximate bridged dinuclear complexes (**1** and **2**) display distorted trigonal bipyramidal geometry and form a six-membered $M_2(NO)_2$ ring oriented in a boat conformation. The two copper(II) centers in **1** interact ferromagnetically giving rise to a triplet-spin ground state whereas the two nickel(II) centers in **2** interact antiferromagnetically to stabilize a singlet-spin state. Variable temperature magnetic susceptibility measurements establish the presence of a weak ferromagnetic coupling (J = 13 cm^{-1}) in **1** and a weak anitiferromagnetic coupling (J = −12 cm^{-1}) in **2**. The exchange coupling constant derived from B3LYP computations in conjunction with broken symmetry spin-projection techniques for the oximate bridged dinuclear copper(II) complex shows excellent agreement with the corresponding experimental value. A square-planar mononuclear nickel(II) complex of the dioxime ligand, $[Ni(H_2L^1)](ClO_4)_2$ (**3**), is reported along with its crystal structure, which reacts with acetonitrile to produce a six-coordinate mononuclear complex, $[Ni(L^2)](ClO_4)_2$ (**4**). The ligand (L^2) in complex **4** is the iminoacyl derivative of oxime, where the coupling of oxime and acetonitrile takes place via a proton-assisted pathway. The iminoacylation of H_2L^1 works with other nitriles like butyronitrile and benzonitrile. Computational studies support a proton-assisted coupling of oxime with nitrile. The critical transition states have been located for the iminoacylation reaction. Complex **4** can be converted back to complex **3** by reacting with sodium acetate in methanol.

Introduction

Exchange coupled polynuclear metal complexes have attracted considerable attention because of their potential application as molecule-based magnetic materials displaying interesting electronic properties.[1−6] Oxime ligands have been widely used for the synthesis of polynuclear spin coupled magnetic molecules.[7] It has been shown that different modes of bindings of oxime ligands can connect transition metal ions generating oximate bridged dinuclear/polynuclear complexes that effectively transmit magnetic exchange coupling.[7,8] The magnetic properties of oximate complexes can easily be tuned by modification on the ligand backbone. The magnetic exchange coupling for a large number of oximate bridged polynuclear metal complexes have been reported in the literature particularly for dicopper(II)[7,9−13] and dinickel(II) complexes.[14,15] The in-plane oximate bridge between magnetic centers in dicopper(II) complexes displays strong antiferromagnetic coupling as a result of effective overlap of magnetic orbitals. On the other hand, out-of-plane oximate bridge reduces the overlap of

*E-mail: ictkp@iacs.res.in. Fax: +91-33-2473-2805. Tel.: +91-33-2473-4971.

(1) Kahn, O. *Molecular Magnetism*; VCH: Weinheim, Germany, 1993.
(2) Gatteschi, D.; Kahn, O.; Miller, J. S.; Palacio, F., Eds. *Magnetic Molecular Materials*; Kluwer Academic Publishers: Dordrecht, The Netherlands, 1991.
(3) O′Connor, C. J., Ed. *Research Frontiers in Magnetochemistry*; World Scientific: Singapore, 1993.
(4) Miller, J. S.; Brillon, M., Eds. *Magnetism: Molecules to Materials*; Wiley-VCH: Weinheim, Germany, 2002.
(5) Gatteschi, D.; Sessoli, R. *Angew. Chem., Int. Ed.* **2003**, *42*, 268.
(6) Christou, G.; Gatteschi, D.; Hendrickson, D. N.; Sessoli, R. *MRS Bull.* **2000**, 66.
(7) Chaudhuri, P. *Coord. Chem. Rev.* **2003**, *243*, 143.
(8) Chaudhuri, P. *Proc. Indian Acad. Sci.* (*Chem. Sci.*) **1999**, *111*, 397.
(9) Prushan, M. J.; Addison, A. W.; Butcher, R. J.; Thompson, L. K. *Inorg. Chim. Acta* **2005**, *358*, 3449.
(10) Ruiz, R.; Sanz, J.; Lloret, F.; Julve, M.; Faus, J.; Bois, C.; Muñoz, M. C. *J. Chem. Soc., Dalton Trans.* **1993**, 3035.
(11) Maekawa, M.; Kitagawa, S.; Nakao, Y.; Sakamoto, S.; Yatani, A.; Mori, W.; Kashino, S.; Munakata, M. *Inorg. Chim. Acta* **1999**, *293*, 20.
(12) Cervera, B.; Ruiz, R.; Lloret, F.; Julve, M.; Cano, J.; Faus, J.; Bois, C.; Mrozinski, J. *J. Chem. Soc., Dalton Trans.* **1997**, 395.
(13) Curtis, N. F.; Gladkikh, O. P.; Heath, S. L.; Morgan, K. R. *Aust. J. Chem.* **2000**, *53*, 577.
(14) Schlemper, E. O.; Murmann, R. K. *Inorg. Chem.* **1974**, *13*, 2424.
(15) Agnus, Y.; Louis, R.; Jesser, R.; Weiss, R. *Inorg. Nucl. Chem. Lett.* **1976**, *12*, 455.

Published on Web 12/21/2009

Chart 1. Ligands Used in This Work

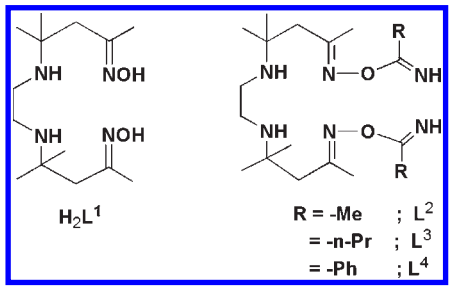

magnetic orbitals and exhibits weak ferro- or antiferromagnetic coupling.

With an aim to study the magnetic properties of exchange coupled oximate bridged metal complexes and to understand their reactivity, we have explored the chemistry of a β-aminoketoxime ligand, 4,4,9,9-tetramethyl-5,8-diazadodecane-2,11-dione dioxime (H_2L^1) (Chart 1). The dioxime ligand (H_2L^1) was first reported by Powell and co-workers in 1970[16] and have shown the coordination of oxime ligand with iron(II), copper(II), nickel(II), and zinc(II) ions.[17,18] Schlemper and co-workers have prepared and structurally characterized a monomeric octahedral Rh(III) complex $[Rh(HL^1)Cl_2]$, as a model compound for the study of potential radiopharmaceutical.[19] Powell and co-workers have reported the synthesis of copper(II) complexes of the oxime ligand and the solid-state structure of an oximate bridged dimeric copper(II) complex, $[Cu_2(HL^1)_2]Br_2$, where the $Cu_2(NO)_2$ ring adopts a boat conformation.[17] However, they did not report the variable-temperature magnetic study of the complex. In the dimeric copper(II) complex, the oxime ligand exhibits out-of-plane bridging and is expected to show interesting magnetic properties. In this paper, we describe the syntheses, structures, and magnetic properties of the dimeric copper(II) complex $[Cu_2(HL^1)_2](ClO_4)_2$ (**1**), its nickel(II) analog $[Ni_2(HL^1)_2](ClO_4)_2$ (**2**), and a mononuclear nickel(II) complex $[Ni(H_2L^1)](ClO_4)_2$ (**3**) of dioxime H_2L^1. We also report herein an unexpected coupling of the dioxime ligand with nitriles mediated by nickel(II) ion and concomitant formation of nickel(II) complexes of the iminoacylated ligands (L^{2-4} in Chart 1). Kukushkin and others have reported this kind of coupling with some ketoximes, aldoximes, chloroximes, amidoximes, and *vic*-dioximes,[20,21] mediated by metal ions like, vanadium(IV),[22,23] palladium(II),[24] platinum(II),[25] platinum(IV),[26−31] rhenium(IV),[32] and rhodium(III).[33,34] The oxime−nitrile coupling reaction templated by nickel(II) ion for a thioether-oxime ligand is reported.[35,36] In all cases, the attack of coordinated nitrile by oxime has been proposed but there is little mechanistic information reported in the literature. Here, we report a proton-assisted iminoacylation of oxime H_2L^1 during the conversion of **3** (or **2**) to **4**. The crystal structure of one six-coordinate nickel(II) complex of iminoacylated ligand L^2, $[NiL^2](ClO_4)_2$ (**4**) along with its conversion to oxime complex **3** is reported in this work.

Experimental Section

Commercial grade chemicals were used for synthetic purposes and distilled solvents were used. *Caution: Although no problems were encountered during the synthesis of the ligand and the complex, perchlorate salts are potentially explosive and should be handled with care!*[37] The oxime derivative (H_2L^1) of 4,4,9,9-tetramethyl-5,8-diazadodecane-2,11-dione was synthesized according to a literature procedure.[16]

$[Cu_2(HL^1)_2](ClO_4)_2$ (1). To a suspension of the ligand H_2L^1 (0.286 g, 1 mmol) in 25 mL of MeOH was added $Cu(ClO_4)_2\cdot 6H_2O$ (0.37 g, 1 mmol) and the reaction mixture was stirred at room temperature for 10 h. The resulting blue solution was filtered to remove any insoluble impurities. The solution was allowed to evaporate slowly at room temperature to isolate a green crystalline solid suitable for X-ray diffraction. Yield: 0.37 g (83%). Anal calcd for $C_{28}H_{58}Cl_2Cu_2N_8O_{12}$: C, 37.50; H, 6.52; N, 12.49. Found: C, 37.3; H, 6.4; N, 12.0. IR (KBr, cm^{-1}): 3570 (s), 3465 (s), 3217 (s), 2970−2887 (br), 1631(m), 1463 (m), 1427 (m), 1377 (s), 1244 (s), 1143−1089 (vs), 630 (s). Λ (mho cm^2 mol^{-1} in MeOH): 185. ESI-MS (positive ion mode, MeCN): m/z = 348.22 (100%, $[(HL^1)Cu]^+$), 276.16 (75%, $[(HL^1)Cu-C_3H_6NO]^+$) . UV−vis in MeCN (λ, nm; ε, $M^{-1}cm^{-1}$): 586 (350), 372 (1750).

$[Ni_2(HL^1)_2](ClO_4)_2$ (2). To a suspension of ligand (0.286 g, 1 mmol) in 15 mL MeOH, a mixture of $NiCl_2\cdot 6H_2O$ (0.236 g, 1 mmol) and $NaClO_4\cdot H_2O$ (0.28 g, 2 mmol) in 10 mL MeOH was added. The mixture was allowed to stir for 12 h at room temperature to form an orange solution. The solution was filtered and the solvent was evaporated slowly to get an orange reaction mixture. The mixture was redissolved in MeOH to prepare a very dilute solution. Deep green rhombic shaped crystals, suitable for X-ray single crystal diffraction, were isolated by vapor diffusion of diethyl ether into the dilute methanolic solution of the mixture. Yield: 0.27 g (61%). Anal calcd for $C_{28}H_{58}Cl_2N_8Ni_2O_{12}$: C, 37.91; H, 6.59; N, 12.63. Found: C, 37.9; H, 6.2; N, 12.2. IR (KBr, cm^{-1}): 3234 (s), 2970−2881 (s),

(16) Fraser, J. W.; Hedwig, G. R.; Morgan, M. M.; Powell, H. K. J. *Aust. J. Chem.* **1970**, *23*, 1847.
(17) Fraser, J. W.; Hedwig, G. R.; Powell, H. K. J.; Robinson, W. T. *Aust. J. Chem.* **1972**, *25*, 747.
(18) Powell, H. K. J.; Russell, J. M. *Aust. J. Chem.* **1978**, *31*, 2409.
(19) Lynde-Kernell, T.; Schlemper, E. O. *J. Coord. Chem.* **1988**, *16*, 347.
(20) Kukushkin, V. Y.; Pombeiro, A. J. L. *Coord. Chem. Rev.* **1999**, *181*, 147.
(21) Kukushkin, V. Y.; Pombeiro, A. J. L. *Chem. Rev.* **2002**, *102*, 1771.
(22) Grigg, J.; Collison, D.; Garner, C. D.; Helliwell, M.; Tasker, P. A.; Thorpe, J. M. *J. Chem. Soc., Chem. Commun.* **1993**, 1807.
(23) Zerbib, V.; Robert, F.; Gouzerh, P. *J. Chem. Soc., Chem. Commun.* **1994**, 2179.
(24) Garnovskii, D. A.; Bokach, N. A.; Pombeiro, A. J. L.; Haukka, M.; Fraústo da Silva, J. J. R.; Kukushkin, V. Y. *Eur. J. Inorg. Chem.* **2005**, 3467.
(25) Ferreira, C. M. P.; Guedes da Silva, M. F. C.; Fraústo da Silva, J. J. R.; Pombeiro, A. J. L.; Kukushkin, V. Y.; Michelin, R. A. *Inorg. Chem.* **2001**, *40*, 1134.
(26) Kukushkin, V. Y.; Pakhomova, T. B.; Kukushkin, Y. N.; Herrmann, R.; Wagner, G.; Pombeiro, A. J. L. *Inorg. Chem.* **1998**, *37*, 6511.
(27) Garnovskii, D. A.; Guedes da Silva, M. F. C.; Pakhomova, T. B.; Wagner, G.; Duarte, M. T.; Fraústo da Silva, J. J. R.; Pombeiro, A. J. L.; Kukushkin, V. Y. *Inorg. Chim. Acta* **2000**, *300−302*, 499.
(28) Kuznetsov, M. L.; Bokach, N. A.; Kukushkin, V. Y.; Pakkanen, T.; Wagner, G.; Pombeiro, A. J. L. *J. Chem. Soc., Dalton Trans.* **2000**, 4683.
(29) Kukushkin, V. Y.; Pakhomova, T. B.; Bokach, N. A.; Wagner, G.; Kuznetsov, M. L.; Galanski, M.; Pombeiro, A. J. L. *Inorg. Chem.* **2000**, *39*, 216.
(30) Makarycheva-Mikhailova, A. V.; Haukka, M.; Bokach, N. A.; Garnovskii, D. A.; Galanski, M.; Keppler, B. K.; Pombeiro, A. J. L.; Kukushkin, V. Y. *New J. Chem.* **2002**, *26*, 1085.
(31) Garnovskii, D. A.; Pombeiro, A. J. L.; Haukka, M.; Sobota, P.; Kukushkin, V. Y. *Dalton Trans.* **2004**, 1097.
(32) Wagner, G.; Pombeiro, A. J. L.; Bokach, N. A.; Kukushkin, V. Y. *J. Chem. Soc., Dalton Trans.* **1999**, 4083.
(33) Kukushkin, V. Y.; Ilichev, I. V.; Wagner, G.; Fraústo da Silva, J. J. R.; Pombeiro, A. J. L. *J. Chem. Soc., Dalton Trans.* **1999**, 3047.
(34) Kukushkin, V. Y.; Ilichev, I. V.; Zhdanova, M. A.; Wagner, G.; Pombeiro, A. J. L. *J. Chem. Soc., Dalton Trans.* **2000**, 1567.
(35) Pavlishchuk, V. V.; Kolotilov, S. V.; Addison, A. W.; Prushan, M. J.; Butcher, R. J.; Thompson, L. K. *Inorg. Chem.* **1999**, *38*, 1759.
(36) Pavlishchuk, V. V.; Kolotilov, S. V.; Addison, A. W.; Prushan, M. J.; Butcher, R. J.; Thompson, L. K. *Chem. Commun.* **2002**, 468.
(37) Wolsey, W. C. *J. Chem. Educ.* **1973**, *50*, A335.

1630 (m), 1465−1423, 1371 (s), 1280, 1164 (s), 1093 (vs), 999 (s), 947 (m), 856 (m), 783, 622 (s). Λ (mho cm^2 mol^{-1} in MeOH): 161. ESI-MS (positive ion mode, MeOH): m/z = 342.97 (100%, $[(HL^1)Ni]^+$). UV−vis in MeOH (λ, nm; ε, $M^{-1}cm^{-1}$):, 482 (600), 312 (5800).

$[Ni(H_2L^1)](ClO_4)_2$ (3). The orange reaction mixture was obtained as described for the synthesis of complex **2**. The mixture was redissolved in MeOH to prepare a very concentrated solution. Deep orange single crystals, suitable for X-ray structure determination, were isolated by slow vapor diffusion of diethyl ether into the concentrated methanolic solution of the mixture. Yield: 0.28 g (51%). Anal calcd for $C_{14}H_{30}Cl_2N_4NiO_{10}$: C, 30.91; H, 5.56; N, 10.30. Found: C, 30.6; H, 5.5; N, 10.8. IR (KBr, cm^{-1}): 3450 (br), 3265 (s), 3180 (m), 2974−2880 (s), 1633 (s), 1465 (m), 1431(m), 1375 (s), 1260 (m), 1144−1088 (vs), 1002 (s), 933 (m), 850 (m), 770 (m), 625 (s). Λ (mho cm^2 mol^{-1} in MeOH): 127. ESI-MS (positive ion mode, MeOH): m/z = 343.25 (100%, $[(HL^1)Ni]^+$), 287.32 (8%, $[H_2L^1 + H]^+$). UV−vis in MeOH (λ, nm; ε, M^{-1} cm^{-1}): 482 (340), 312 (3100).

$[NiL^2](ClO_4)_2$ (4). To a suspension of ligand (0.144 g, 0.5 mmol) in 15 mL MeCN, a mixture of $NiCl_2\cdot 6H_2O$ (0.118 g, 0.5 mmol) and $NaClO_4\cdot H_2O$ (0.14 g, 1 mmol) in 10 mL MeCN were added. The pink solution was stirred for 12 h at room temperature. X-ray quality pink crystals were obtained by slow evaporation of the reaction solution. Yield: 0.17 g (54%). Anal calcd for $C_{18}H_{36}Cl_2N_6NiO_{10}$: C, 34.53; H, 5.80; N, 13.42. Found: C, 34.6; H, 5.5; N, 13.0. IR (KBr, cm^{-1}): 3321 (s), 3276 (s), 2975 (m), 1687 (s), 1647 (s), 1442(m), 1394 (s), 1144−1092(vs), 922 (m), 860 (w), 625 (s). Λ (mho cm^2 mol^{-1} in MeOH): 163. ESI-MS (positive ion mode, MeCN): m/z = 525.23 (10%, $[L^2Ni + ClO_4]^+$), 343.19 (100%, $[(L^2Ni - C_4H_8N_2) + H]^+$), 325.19 (15%, $[(L^2Ni-C_4H_9N_2O)]^+$). UV−vis in MeOH (λ, nm; ε, M^{-1} cm^{-1}): 890 (23), 795 (sh), 490 (46), 312 (sh).

$[NiL^3](ClO_4)_2$ (5). To a methanolic (20 mL) solution of ligand (0.286 g, 1 mmol) was added a mixture of $NiCl_2\cdot 6H_2O$ (0.236 g, 1 mmol) and $NaClO_4\cdot H_2O$ (0.28 g, 2 mmol) in MeOH. To the red reaction solution, butyronitrile (0.218 mL, 2.5 mmol) was added and the solution was allowed to stir for 24 h at room temperature. The resulting pink solution was filtered, and the filtrate was slowly evaporated to dryness to get a pink gum. The gum was redissolved in a mixture of MeOH and butyronitrile (5:1) and was kept for slow vapor diffusion of ether into the solution to isolate pink crystalline solid of complex **5**. Yield: 0.14 g (20%). Anal calcd for $C_{22}H_{44}Cl_2N_6NiO_{10}$: C, 38.73; H, 6.50; N, 12.32. Found: C, 38.8; H, 6.2; N, 12.3. IR (KBr, cm^{-1}): 3305 (s), 3269 (s), 2974−2941 (m), 1680 (s), 1643 (s), 1463 (m), 1419−1398 (s), 1276, 1149−1090 (vs), 989 (m), 929 (m), 623 (s). Λ (mho cm^2 mol^{-1} in MeOH): 164. ESI-MS (positive ion mode, MeOH): m/z = 383.33 (5%, $[L^3Ni - C_4H_8N_2O]^+$), 343.28 (100%, $[L^3Ni - C_8H_{15}N_2]^+$). UV−vis in MeOH (λ, nm; ε, M^{-1} cm^{-1}): 890 (27), 800 (sh), 525 (25), 310 (sh).

$[NiL^4](ClO_4)_2$ (6). To a mixture of $NiCl_2\cdot 6H_2O$ (0.236 g, 1 mmol) and $NaClO_4\cdot H_2O$ (0.28 g, 2 mmol) in 20 mL MeOH, ligand H_2L^1 (0.286 g, 1 mmol) was added. To that benzonitrile (2.53 mL, 25 mmol) was added and the reaction mixture was refluxed for 2 h. The light pink solution was further stirred at room temperature for 2 d. The solution was then filtered to remove any insoluble impurity, and the filtrate was evaporated slowly. A purple compound was obtained, which was washed with diethyl ether and the solid was kept under vacuum for 2 h to get a purple solid. Yield: 0.23 g (31%). Anal calcd for $C_{28}H_{40}Cl_2N_6NiO_{10}$: C, 44.82; H, 5.37; N, 11.20. Found: C, 45.0; H, 5.4; N, 11.3. IR (KBr, cm^{-1}): 3317 (s), 3269 (s), 2975 (m), 1670 (s), 1637 (s), 1450 (m), 1377 (s), 1278, 1205 (m), 1093 (vs), 935 (s), 781 (m), 696 (s), 623(s). Λ (mho cm^2 mol^{-1} in CH_3OH): 164. ESI-MS (positive ion mode, MeOH): m/z = 648.92 (10%, $[L^5Ni + ClO_4]^+$), 343.02 (100%, $[L^5Ni - C_{14}H_{11}N_2]^+$). UV−vis in MeOH ($\lambda$, nm; ε, M^{-1} cm^{-1}): 890 (33), 798 (30), 500 (53), 315 (sh).

Conversion of 3 to 4. A 16.8 mg (0.03 mmol) portion of complex **3** was dissolved in 2 mL MeCN and the solution was allowed to stand at room temperature for 7 d. The pink-red solution was then kept for slow vapor diffusion of diethyl ether. A purple crystalline solid of complex **4** was isolated after several days. Yield: 6 mg (30%). Further ether diffusion into the filtrate produced green complex **2**.

Physical Measurements. Fourier transform infrared spectroscopy on KBr pellets was performed on a Shimadzu FT-IR 8400S instrument. Elemental analyses were performed on a Perkin-Elmer 2400 series II CHN series. Solution electronic spectra were measured on an Agilent 8453 diode array spectrophotometer. Electro-spray mass spectra were recorded with Waters QTOF Micro YA263. Magnetic susceptibilities of the polycrystalline sample were recorded on a SQUID magnetometer (MPMS, Quantum Design) in the temperature range 2−290 K with an applied field of 1 T. Experimental susceptibility data were corrected for the underlying diamagnetism using Pascal's constant. The program julX written by E. Bill was used for the simulation and analysis of magnetic susceptibility data calculating through full-matrix diagonalization of the Spin-Hamiltonian.[38] Solution conductivity measurements were carried out in acetonitrile solution at room temperature on a Systronics Conductivity Meter 306. Thermogravimetric analysis (TGA) measurements were carried out on a TA Instruments SDT Q 600 thermal analyzer.

X-ray Crystal Structure Determination. Crystallographic data for **1**−**4** are summarized in Table 1. X-ray single crystal data were collected using Mo Kα (λ = 0.7107 Å) radiation on a SMART APEX diffractometer equipped with charge-coupled device (CCD) area detector. Data collection, data reduction, and structure solution/refinement were carried out using the software package of APEX II.[39] All structures were solved by direct method and refined in a routine manner. In most of the cases, non-hydrogen atoms were treated anisotropically. Whenever possible, the hydrogen atoms were located on a difference Fourier map and refined. In other cases, the hydrogen atoms were geometrically fixed. In complexes **1** and **2**, at the end of the refinement cycles, some disordered electron densities were located in the asymmetric unit. SQUEEZE[40] calculations indicated the presence of 95 and 130 electrons per unit cell for complex **1** and **2**, respectively. The disordered perchlorate counterions in complexes **1**−**3** were refined isotropically using the second free variable facility (FVAR) provided with SHELXTL,[41] so the total site occupancy factor (SOF) of the disordered atom is one.

Theoretical Calculation. Molecular geometries were optimized using the B3LYP functional,[42−45] as implemented in the Gaussian 03 quantum chemistry suite of programs.[46] All stationary points obtained were characterized using full Hessian matrix computation with all real frequencies for the minima and a single imaginary frequency for the transition states. Intrinsic reaction coordinate studies were performed to connect the transition states with their corresponding reactant and product states. Zero-point energies were determined for optimized molecular geometries and the total energies were zero-point corrected. For the coupling constant computations, 6-31G(d, p)

(38) Bill, E. julX Program; Max-Planck-Institut für Bioanorganische Chemie: Mülheim an der Ruhr, Germany, 2008.
(39) *Bruker*, 2.1−0 ed.; Bruker AXS inc.: Madison, WI, 2006.
(40) van der Sluis, P.; Spek, A. L. *Acta Crystallogr.* **1990**, *A46*, 194.
(41) Sheldrick, G. M. *SHELXTL NT*, version 5.1, Program for Solution and Refinement of Crystal Structures; University of Göttingen: Germany, 1997.
(42) Stephens, P. J.; Devlin, F. J.; Chabalowski, C. F.; Frisch, M. J. *J. Phys. Chem.* **1994**, *98*, 11623.
(43) Becke, A. D. *Phys. Rev. A* **1988**, *38*, 3098.
(44) Becke, A. D. *J. Chem. Phys.* **1993**, *98*, 5648.
(45) Lee, C.; Yang, W.; Parr, R. *Phys. Rev. B* **1988**, *37*, 785.
(46) Frisch, M. J. et al. *Gaussian 03*, revision C.02; Gaussian Inc.: Wallingford, CT, 2004; the full citation is in the Supporting Information.

Table 1. Crystallographic Data for Complexes **1**−**4**

crystal parameters	1	2	3	4
empirical formula	$C_{28}H_{58}Cl_2\ Cu_2N_8O_{12}$	$C_{28}H_{58}Cl_2N_8Ni_2O_{12}$	$C_{14}H_{30}Cl_2N_4NiO_{10}$	$C_{18}H_{36}Cl_2N_6NiO_{10}$
formula weight	896.80	887.14	544.03	626.14
crystal system	monoclinic	monoclinic	orthorhombic	orthorhombic
space group	*C*2/*c*	*C*2/*c*	*Fdd*2	*Pbca*
a/Å	20.415(3)	20.444(5)	13.8825(11)	16.8663(6)
b/Å	14.1343(19)	14.148(3)	38.280(3)	13.5170(5)
c/Å	16.694(2)	16.923(4)	8.3526(7)	23.7460(8)
α/deg	90.00	90.00	90.00	90.00
β/deg	104.673(3)	104.958(6)	90.00	90.00
γ/deg	90.00	90.00	90.00	90.00
volume/Å^3	4659.9(10)	4729(2)	4438.8(6)	5413.7(3)
Z	4	4	8	8
D_{calc}/g cm^{-3}	1.278	1.246	1.628	1.536
F(000)	1880	1872	2272	2624
μ Mo Kα /mm^{-1}	1.083	0.964	1.173	0.975
temperature/K	298(2)	298(2)	100(2)	150(2)
R_{int}	0.0392	0.0607	0.0326	0.0591
range of *h*, *k*, *l*	−24/24, −16/16, −19/19	−22/22, −15/15, −18/18	−17/18, −55/54, −10/12	−22/ 22, −17/ 17, −31/31
θ min/max/deg	1.77/24.98	1.77/23.49	2.13/31.07	1.72/28.16
reflections collected/unique/ observed [$I > 2\sigma(I)$]	21193/4067/3270	19151/3468/2640	12784/2965/2594	55029/6587/4955
data/restraints/parameters	4067/1/246	3468/0/245	2965/1/145	4955/0/358
goodness of fit on F^2	1.095	1.069	1.037	1.009
final *R* indices	$R_1 = 0.0477$	$R_1 = 0.0528$	$R_1 = 0.0514$	$R_1 = 0.0348$
[$I > 2\sigma(I)$]	$wR_2 = 0.1416$	$wR_2 = 0.1442$	$wR_2 = 0.1311$	$wR_2 = 0.0814$
R indices	$R_1 = 0.0622$	$R_1 = 0.0731$	$R_1 = 0.0595$	$R_1 = 0.0569$
(all data)	$wR_2 = 0.1517$	$wR_2 = 0.1581$	$wR_2 = 0.1362$	$wR_2 = 0.0912$

basis sets were used for all the atoms. However, for the computations related to reaction mechanism investigations which involved optimization of relevant molecular structures of intermediates and transition states, LANL2DZ for nickel was employed[47−49] and 6-31G(d) basis sets were used for all other atoms. The solution phase total energies were computed by using the CPCM variant of the self-consistent reaction field model[50,51] with acetonitrile as the solvent along with LANL2DZ for nickel, the Pople 6-31G(d,p) basis sets were used for all other atoms . The exchange coupling constants were computed using the X-ray characterized structures, and the broken symmetry manifold (developed by Noodleman et al.[52]) along with spin-projection techniques of Ruiz and co-workers were employed.[53] Wave function stability analysis was carried out to verify if the broken symmetry wave function has converged to the desired electronic state.

Results and Discussion

Complex **1** is synthesized by reacting H_2L^1 with $Cu(ClO_4)_2\cdot 6H_2O$ in methanol at room temperature (Scheme 1).[17] The reaction of H_2L^1 with $NiCl_2\cdot 6H_2O$ and $NaClO_4\cdot H_2O$ in methanol at ambient condition gives the dimeric Ni(II) complex **2**, which is crystallized by vapor diffusion of diethyl ether into a dilute methanolic reaction mixture. The mononuclear oxime complex $[Ni(H_2L^1)](ClO_4)_2$ (**3**) is isolated by vapor diffusion of diethyl ether into a concentrated methanolic solution of the reaction mixture. Interestingly, when H_2L^1 is reacted with $NiCl_2\cdot 6H_2O$ and $NaClO_4\cdot H_2O$ in acetonitrile at room temperature, a mononuclear complex $[NiL^2](ClO_4)_2$ (**4**) is isolated. During the reaction in acetonitrile, ligand H_2L^1 gets modified

Scheme 1. Syntheses of Complexes **1**−**6**

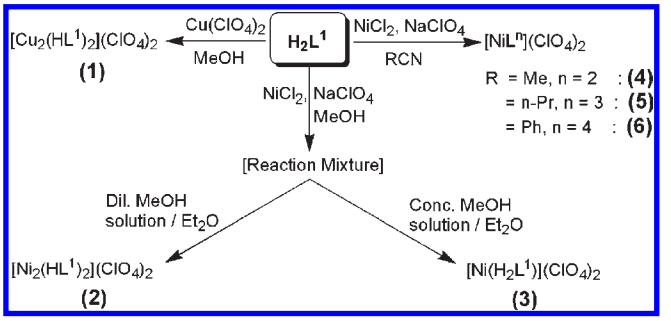

through a nickel(II) templated oxime−nitrile coupling to form iminoacylated ligand L^2. The iminoacylation reaction of oxime is also observed, but with relatively low yield, for butyronitrile and benzonitrile to form complexes **5** and **6**, respectively.

In the IR spectra of all the complexes, strong and broad bands are observed in the region 1150−1080 cm^{-1} and at around 625 cm^{-1}, that correspond to perchlorate counterion. The band at around 1630 cm^{-1} for complexes **1**−**3** can be assigned to the oxime C=N stretching vibrations and is shifted to higher energy in complexes **4**−**6**. Other C=N stretching frequencies are observed for complexes **4**−**6** in the region 1670−1690 cm^{-1}. All the complexes show strong and sharp bands for N−H stretching from the ligand backbone in the region 3215−3275 cm^{-1}. Additionally complexes **4**−**6** show strong and sharp peaks in the region 3305−3325 cm^{-1}, not present in the dioxime ligand, indicating that the ligand underwent transformation to form iminoacyl derivatives of oxime. Solution conductivity measurements in methanol at room temperature for all the complexes indicate 1:2 electrolyte complexes with an exception in complex **3**.[54] The low conductivity of **3** in methanol indicates the interaction of perchlorate anion with the metal center or with

(47) Hay, P. J.; Wadt, W. R. *J. Chem. Phys.* **1985**, *82*, 270.
(48) Hay, P. J.; Wadt, W. R. *J. Chem. Phys.* **1985**, *82*, 284.
(49) Hay, P. J.; Wadt, W. R. *J. Chem. Phys.* **1985**, *82*, 299.
(50) Barone, V.; Cossi, M. *J. Phys. Chem. A* **1998**, *102*, 1995.
(51) Cossi, M.; Rega, N.; Scalmani, G.; Barone, V. *J. Comput. Chem.* **2003**, *24*, 669.
(52) Noodleman, L. *J. Chem. Phys.* **1981**, *74*, 5737.
(53) Ruiz, E.; Cano, J.; Alvarez, S.; Alemany, P. *J. Comput. Chem.* **1999**, *20*, 1391.
(54) Geary, W. J. *Coord. Chem. Rev.* **1971**, *7*, 81.

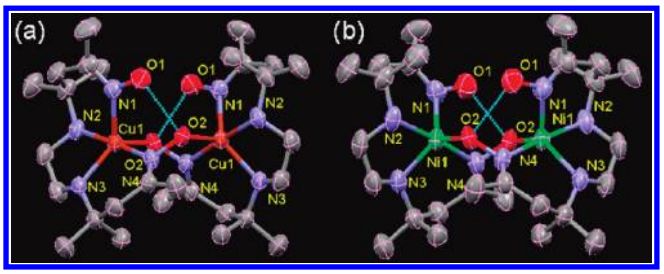

Figure 1. Thermal ellipsoid plot of (a) the cationic complex **1** and (b) the cationic complex **2**. Intramolecular hydrogen bonding interactions involving oxime hydroxyl group and bridging oximate oxygen atom are shown by dotted lines with thermal ellipsoid drawn at the 50% probability level.

another molecule in solution. Electrospray ionization mass spectrometry (ESI-MS) for **1** and **2** show molecular ion peaks at *m*/*z* 348.22 and 342.97, respectively, with expected isotope distribution patterns calculated for $[(HL^1)Cu]^+$ and $[(HL^1)Ni]^+$, respectively. This indicates that the dimeric structure of **1** and **2** is not retained in solution and the corresponding monomers are formed in the mass spectroscopic condition. The mass spectral pattern for complex **3** is found to be similar to that observed in complex **2**. ESI-MS of **4** and **6** show molecular ion peaks at *m*/*z* 525.23 and 648.92 with expected isotope distribution patterns calculated for $[L^2Ni + ClO_4]^+$ and $[L^4Ni + ClO_4]^+$, respectively. While no molecular ion peak is observed for complex **5**, all the iminoacyl complexes (**4**−**6**) show major peak at *m*/*z* 343.20 attributable to $[(HL^1)Ni]^+$. This fragment is formed during the ionization process of ESI-MS measurement. The optical spectrum of complex **1** shows transitions at 586 and 382 nm that can be assigned to d−d band and oximate-to-copper(II) charge transfer band, respectively. The nickel(II) complexes (**2** and **3**) show very similar optical spectra with d−d transition at 482 nm and oximate-to-nickel(II) charge transfer transition at 312 nm in methanol. This suggests that the dimeric species **2** is in equilibrium with monomeric species **3** in solution. In acetonitrile, the position of charge-transfer band shifts to 325 nm whereas the d−d band shifts to 475 nm. All the three six-coordinate nickel(II) complexes **4**−**6** show d−d transitions at around 890, 800, and 525 nm. The ligand field strength, calculated from solution optical spectral $^3A_{2g} \rightarrow {}^3T_{2g}$ transition, for all iminoacylated ligands were found to be around 11 000 cm^{-1}.

Crystal Structures for Complexes $[Cu_2(HL^1)_2](ClO_4)_2$ (1) and $[Ni_2(HL^1)_2](ClO_4)_2$ (2). Crystals of both **1** and **2** belong to monoclinic centrosymmetric space group *C*2/*c* with same unit-cell dimensions and the positions of atoms except for a replacement of copper in **1** with nickel in **2** (Table 1). The asymmetric unit of both of them is comprised of a half of the complex $[M(HL^1)]$ located on a center of inversion and a perchlorate counteranion. In the complexes, each metal ion is coordinated by two imine nitrogens, two amine nitrogens, and one oximate oxygen of another ligand (Figure 1). The metal center displays a slightly distorted trigonal bipyramidal geometry (τ = 0.85 for **1** and τ = 0.80 for **2**).[55] The equatorial planes at the metal centers are occupied by one imine nitrogen N(1), one amine nitrogen N(3), and the coordinated oximate oxygen atom O(2) of other ligand with bond

(55) Addison, A. W.; Rao, T. N.; Reedijk, J.; Rijn, J.; Verschoor, G. C. *J. Chem. Soc., Dalton Trans.* **1984**, 1349.

Table 2. Selected Bond Distances (Å) and Angles (deg) for $[M_2(HL^1)_2](ClO_4)_2$ [M = Cu (**1**) and Ni (**2**)]

	1	**2**
M(1)−N(1)	2.124(3)	2.056(4)
M(1)−N(2)	2.043(3)	2.092(4)
M(1)−N(3)	2.065(3)	2.075(4)
M(1)−N(4)	1.973(3)	2.022(4)
M(1)−O(2)	2.083(2)	1.972(3)
N(1)−O(1)	1.392(4)	1.396(5)
N(4)−O(2)	1.375(4)	1.388(4)
N(1)−M(1)−N(2)	91.79(13)	91.44(16)
N(2)−M(1)−N(3)	85.03(13)	84.47(16)
N(3)−M(1)−N(4)	92.78(12)	91.12(15)
N(4)−M(1)−N(1)	91.01(12)	90.83(15)
N(4)−M(1)−O(2)	92.99(11)	94.45(13)
N(1)−M(1)−N(3)	125.11(12)	115.90(17)
O(2)−M(1)−N(2)	86.81(12)	87.95(14)
N(2)−M(1)−N(4)	177.11(13)	175.57(16)
O(2)−M(1)−N(3)	126.08(12)	127.36(16)
O(2)−M(1)−N(1)	108.33(11)	116.30(14)

distances of M(1)−N(1), M(1)−N(3), and M(1)−O(2) at 2.124(3), 2.065(3), and 2.083(2) Å, respectively, for **1** and at 2.056(4), 2.075(4), and 1.972(3) Å, respectively for **2** (Table 2). The apical sites are coordinated with one amine N(2) and one imine nitrogen N(4) from the ligand having bond distances of M(1)−N(2) and M(1)−N(4) at 2.043(3) and 1.973(3) Å, respectively for **1**, and 2.092(4) and 2.022(4) Å, respectively for **2**. The distortion in trigonal bipyramidal geometry is evident in the deviation of bond angles in equatorial plane from 120° (Table 2). Two apical nitrogens N(2) and N(4) make an angle of 177.11(13)° at the copper(II) center of **1** and of 175.57(16)° at the nickel(II) center of **2**, implying distortion at the metal centers.

In the complexes, the dimeric unit forms a six-membered $M_2(NO)_2$ boatlike cyclic conformation with two oximate O(2) and two imino N(4) of two ligands. The bond parameters and a boat conformation of the $M_2(NO)_2$ core in **1** are very similar to those in the cationic complex $[Cu_2(HL^1)_2]Br_2$, reported by Powell and coworkers.[17] A 2-fold symmetry axis passes along *b* axis, through the center of inversion of the mean plane formed by two M(1) and two O(2) atoms. Two metal ions are positioned diagonally on that mean plane at a distance of 3.843 Å in **1** and of 3.748 Å in **2**. Two imine N(4) atoms are situated at one and four position of the boat, and they are about 0.743 and 0.765 Å out of the mean plane of M(1)−O(2)−M(1)−O(2) for **1** and **2**, respectively.

In both the cases, intramolecular hydrogen bonding is evident between oxime and oximate oxygens. The O(1)···O(2) distance of 2.579 Å in **1** is close comparable to that reported in a related copper(II)−oximate complex, $[Cu_2(HL^1)_2]Br_2$ (2.54 Å).[17] The O(1)···O(2) distance is found to be 2.600 Å in **2**. In addition, intermolecular hydrogen bonding are observed between amine nitrogens N(2), N(3), and perchlorate oxygens (Table S1 in the Supporting Information, SI). The perchlorate anion is involved in a weak hydrogen bonding interaction with the amine nitrogen in both **1** and **2** via N−H···O resulting in the formation of one-dimensional hydrogen bonded polymeric network (Figure S1 in the SI).

In complexes **1** and **2**, at the end of the refinement cycles, some disordered electron densities were located in the asymmetric unit. SQUEEZE[40] calculations indicated

Figure 2. Thermal ellipsoid plot of cationic part of the mononuclear nickel(II) complex (**3**) with thermal ellipsoid drawn at the 50% probability level. Intramolecular hydrogen bonding interaction involving oxime hydroxyl groups is shown by dotted lines.

the presence of 95 and 130 electrons per unit cell or 23.75 and 32.5 electrons per asymmetric unit for **1** and **2**, respectively. This is equivalent to 2.37 and 3.25 molecules of water in **1** and **2**, respectively. Thermogravimetric (TG) data of **1** shows a weight loss of 6.3% in the temperature range of 27−159 °C, which is comparable with SQUEEZE result (calc weight loss for 2.37 H_2O = 4.5%) (Figure S2 in the SI). On the other hand, thermogravimetric data of **2** shows a weight loss of 6.0% in the temperature range of 29−192 °C, which corroborates well with the SQUEEZE result (calc. weight loss for 3.25 H_2O = 6.2%) (Figure S3 in the SI). The large numbers of disordered electrons do not correspond to any counterion (perchlorate). Additionally, the bond valence sum (BVS) analysis[56,57] of the single-crystal data gives the values of 2.10 and 1.83 for **1** and **2**, respectively. These results clearly suggest that the ligand is monoanionic in the dimers and the metal centers are in +2 oxidation state.

Crystal Structure of Complex $[Ni(H_2L^1)](ClO_4)_2$ (3). Complex **3** is a mononuclear tetracoordinated nickel(II) complex and crystallized in a noncentrosymmetric orthorhombic space group *Fdd*2 (Table 1). The metal ion, coordinated by two imine nitrogens N(1) and two amine nitrogens N(2) donor atoms from the ligand backbone, is in a distorted square-planar coordination environment (Figure 2). The asymmetric unit of **3**, comprised of a half of the complex $Ni(H_2L^1)$, is located on a 2-fold axis and a perchlorate counteranion.

The N(1)−O(1) bond distance of 1.414(4) Å is indicative of the presence of oxime groups in the molecule (Table 3). The metal−nitrogen bond angles are almost equal, but a slight distortion is present in the square planar geometry.[58] This reflects in the unequal adjacent bond angles in N(1)−Ni(1)−N(1) (94.17(19)°) and N(2)−Ni(1)−N(2) (87.4(2)°). An intramolecular hydrogen bonding occurs in between two oxime oxygens (O···O = 2.814 Å). The disordered perchlorate anion

(56) Brown, I. D.; Altermatt, D. *Acta Crystallogr.* **1985**, *B41*, 244.
(57) Hati, S.; Datta, D. *J. Chem. Soc., Dalton Trans.* **1995**, 1177.
(58) Daniel, E. A.; March, F. C.; Powell, H. K. J.; Robinson, W. T.; Russell, J. M. *Aust. J. Chem.* **1978**, *31*, 723.

Table 3. Selected Bond Distances (Å) and Angles (deg) for $[Ni(H_2L^1)](ClO_4)_2$ (**3**)

N(1)−O(1)	1.414(4)
N(1)−Ni(1)	1.900(3)
N(2)−Ni(1)	1.925(3)
N(1)−Ni(1)−N(2)	91.01(13)
N(1)−Ni(1)−N(1)	94.17(19)
N(2)−Ni(1)−N(2)	87.4(2)

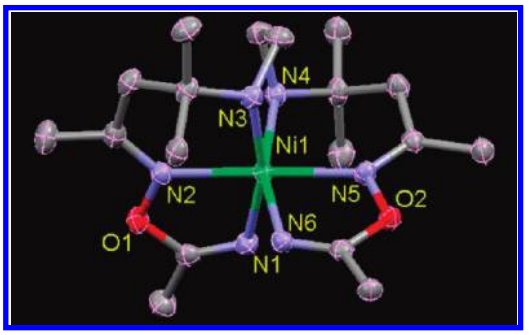

Figure 3. Thermal ellipsoid plot of the mononuclear complex (**4**) with thermal ellipsoid drawn at the 50% probability level.

Table 4. Selected Bond Distances (Å) and Angles (deg) for $[NiL^2](ClO_4)_2$ (**4**)

Ni(1)−N(1)	2.047(2)
Ni(1)−N(2)	2.096(18)
Ni(1)−N(3)	2.106(19)
Ni(1)−N(4)	2.141(18)
Ni(1)−N(5)	2.090(18)
Ni(1)−N(6)	2.084(2)
C(1)−N(1)	1.268(3)
C(17)−N(6)	1.266(3)
N(1)−Ni(1)−N(2)	75.81(7)
N(2)−Ni(1)−N(3)	88.44(7)
N(1)−Ni(1)−N(3)	164.25(8)
N(3)−Ni(1)−N(4)	85.55(7)
N(1)−Ni(1)−N(6)	92.16(8)
N(2)−Ni(1)−N(6)	104.85(7)
N(4)−Ni(1)−N(5)	86.18(7)
N(4)−Ni(1)−N(2)	93.06(7)
N(5)−Ni(1)−N(6)	76.04(7)
N(4)−Ni(1)−N(6)	161.83(8)
N(5)−Ni(1)−N(2)	177.66(7)

is involved in hydrogen bonding with hydroxyl and amine functionality of the ligand via O−H···O and N−H···O interactions (Figure S4 in the SI).

Crystal Structure of Complex $[NiL^2](ClO_4)_2$ (4). Complex **4** is a mononuclear six-coordinate nickel(II) complex (Figure 3) crystallized in a orthorhombic space group *Pbca* (Table 1). The structural analyses revealed that each oxime groups of H_2L^1 has reacted with acetonitrile to form a coupled product with carbon−oxygen covalent bond formation between the nitrile carbon and oxime oxygen. In an octahedral coordination environment, two imine nitrogens N(1) and N(6) from the iminoacylated oxime groups bind to the metal ion in a cis manner, whereas the other two imine nitrogen atoms N(2) and N(5) coordinate in a trans fashion keeping the amine nitrogens N(3) and N(4) cis to each other. This suggests that the oxime ligand has undergone a change in conformation (compared to **3**) during the reaction with acetonitrile. The six Ni−N bonds are almost comparable (within a range of 2.047(2)−2.141(18) Å). The iminoacylation of the oxime groups are confirmed from the bond distances of C(1)−N(1) and C(17)−N(6) at 1.268(3) and 1.266(3) Å, respectively (Table 4).[36] A slight distortion is present in the octahedral geometry which is reflected in

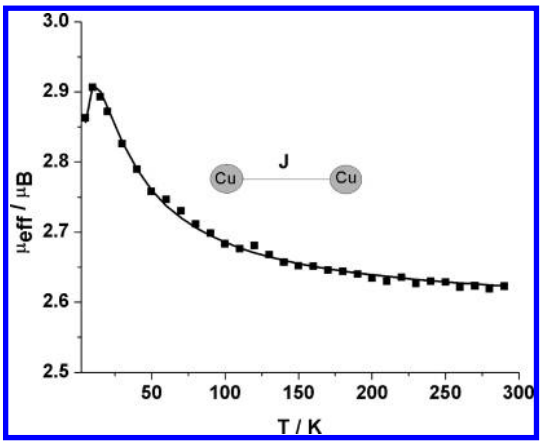

Figure 4. Plot of μ_{eff} (per dimer) vs temperature for complex **1**. The solid line is the theoretical fit of the experimental data.

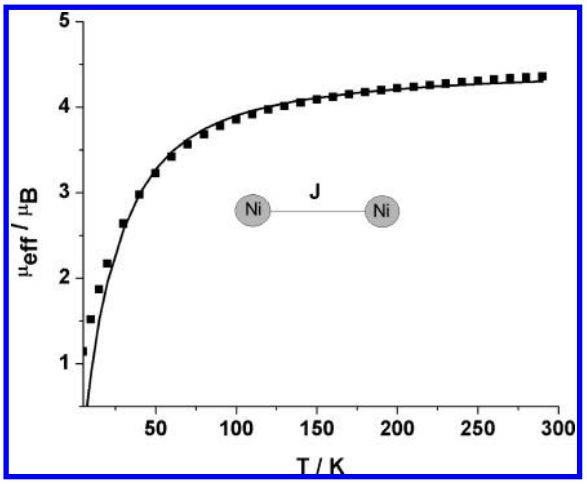

Figure 5. Plot of μ_{eff} (per dimer) vs temperature for complex **2**. The solid line is the theoretical fit of the experimental data.

the bond angles around the metal ion (N(3)−Ni(1)−N(4) and N(1)−Ni(1)−N(6) angles are at 85.55(7)° and 92.16(8)°, respectively). The axial nitrogen donors N(2) and N(5) make a N(5)−Ni(1)−N(2) angle of 177.66(7)° at the nickel center. One of the two perchlorate counteranions is involved in hydrogen bonding with oxime nitrogen atoms of L^2 in the cationic complex via N−H···O [N···O = 2.974(2)−3.152(3) Å] and leads to the formation of a one-dimensional wavelike hydrogen bonded network (Figure S5 in the SI).

Magnetic Studies. The mononuclear nickel(II) complex **3**, being in a square-planar coordination geometry, is diamagnetic. Other mononuclear six-coordinate nickel(II) complexes, **4**−**6**, show effective magnetic moments between 2.80 and 3.00 μ_B (per nickel) at room temperature, as expected for nickel(II) ion in d^8 electronic configuration. The variable temperature magnetic moments for solid samples of dimeric complexes (**1** and **2**) were collected in the temperature range of 5−290 K, and data are shown in Figures 4 and 5. At 290 K, the magnetic moment is 2.61 μ_B for **1** and increases gradually upon cooling to reach the maximum magnetic moment value of 2.91 μ_B at 10 K. Below 10 K, the magnetic moment of **1** decreases further to 2.86 μ_B at 5 K (Figure 4). This behavior is indicative of a ferromagnetic coupling between the copper(II) ions in **1** with some weak intermolecular interaction at low temperature. On the other hand, the dimeric nickel(II) complex **2** shows μ_{eff} value of 4.36 μ_B at 290 K and decreases slowly with lowering the temperature to a magnetic moment value of 1.14 μ_B at 5 K (Figure 5). This nature of temperature dependence of the magnetic moments clearly suggests an antiferromagnetic interaction between the nickel(II) ions in **2**.

The oximate bridged dinuclear complexes, as observed in their structures, form symmetric $M_2(NO)_2$ ring in a boat conformation. The experimental magnetic data were fitted using the exchange-Hamiltonian $\hat{H} = -2J(\hat{S}_1\hat{S}_2)$ ($S_1 = S_2 = 1/2$ for **1** and $S_1 = S_2 = 1$ for **2**) for the dinuclear $M_2(NO)_2$ core. The fitting of the experimental magnetic moment data for **1** gives $J = 13$ cm^{-1}, TIP = 108×10^{-6} emu, $g_{cu} = 2.111$, and the intermolecular exchange parameter $\theta = -0.40$ K (Figure 4). The intermolecular exchange interaction can be explained from the solid state structure of **1** where hydrogen-bonding interaction is operating between the dimeric units through perchlorate ion to form a one-dimensional linear polymeric chain (Figure S1). The J value obtained from the calculated magnetic moment clearly shows a weak ferromagnetic coupling operating in complex **1** giving rise to a triplet-spin ground state.

The fitting of the experimental magnetic moment for dimeric nickel(II) complex **2** yields $J = -12$ cm^{-1}, $g_{Ni} = 2.245$, TIP = 400×10^{-6} emu (Figure 5). Therefore the exchange coupling between the nickel(II) centers through the oximate bridge is weak antiferromagnetic in nature showing the $S = 0$ ground state as observed for reported oximate-bridged dinickel(II) complexes.[14,15]

The exchange coupling constant, J, was computationally determined for the dinuclear copper(II)−oximate complex, **1**. Hybrid density functional computations predict a J value of 14 cm^{-1} which is in excellent agreement with the experimentally determined value of 13 cm^{-1}. For computing the exchange coupling constant, Noodleman's formula[52] was employed:

$$(E_{HS}\text{-}E_{BS})/S_{max}(S_{max}+1)$$

The theoretical study predicts that the ferromagnetically coupled triplet state is indeed slightly more stable than the corresponding antiferomagnetically coupled open-shell singlet state for **1**. Though this excellent agreement between the computationally estimated J and experimentally determined J is somewhat fortuitous, the computational predicted value unequivocally indicates that the triplet (ferromagnetically coupled) and the open shell singlet state (antiferromagnetically coupled) are very close energetically, which is in agreement with the experimental finding. It should be noted for complex **1** the triplet state is single reference in nature and can be treated within the DFT framework. However, for complex **2**, the triplet state itself in principle is multideterminantal in nature, and the converged wave function shows significant spin-contamination. It is not surprising to envision complex **2** comprising two triplet nickel(II) centers which are antiferromagnetically coupled. Only the high-spin quintet can be well-described within the manifold of a single-reference Kohn−Sham density functional theory (DFT). Unfortunately after several attempts, it was not possible to converge the wave function of the

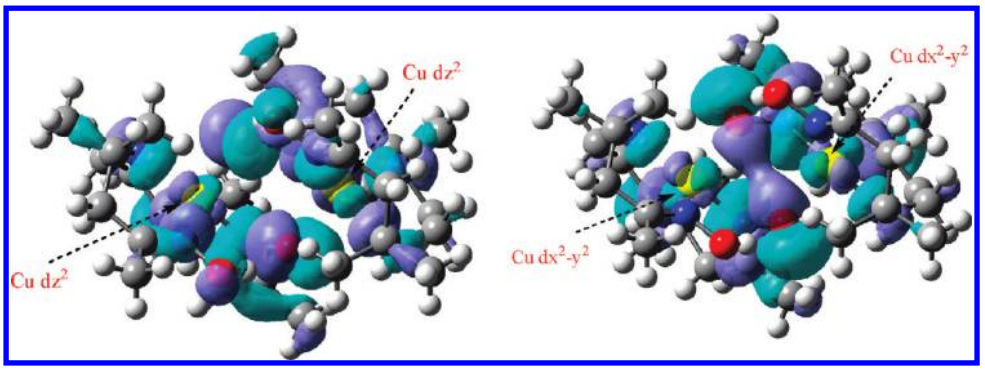

Figure 6. Plots of SOMOs for triplet state of complex **1**.

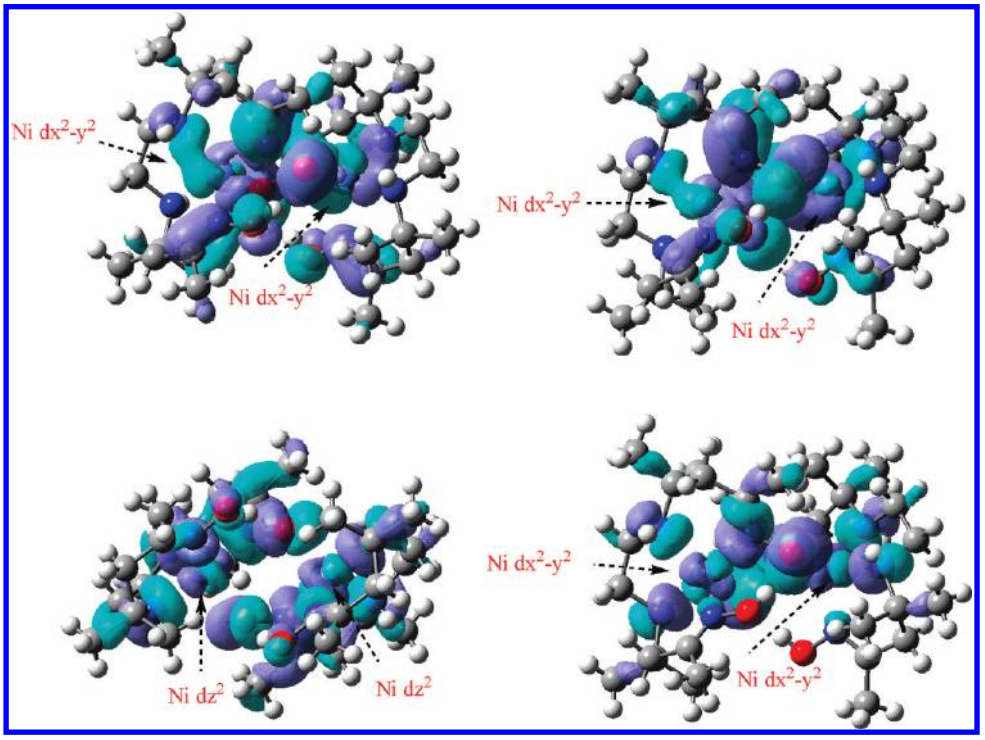

Figure 7. Plots of four SOMOs for the quintet state of complex **2**.

broken-symmetry state for complex **2** to a stable solution. Hence, the exchange-coupling constant for complex **2** could not be determined.

The small ferromagnetic coupling constant is a result of the small energy separation between the triplet ground state and the open shell antiferromganetically coupled singlet state. At a first glance, the molecular geometry of **1** instinctively suggests that the two trigonal bipyramidal paramagnetic copper(II) centers are aligned in such a way that their d-orbitals have minimum overlap resulting in a significant energetic separation between the triplet and the singlet state, with triplet being the ground state. Surprisingly, it was found that such a structural orientation in complex **1** favors a dramatically low energy gap between the antiferromagnetically coupled open shell singlet state and the ferromagnetically coupled triplet state. To understand the origin of this apparent conundrum, the pertinent frontier Kohn−Sham orbitals (those which are responsible for the magnetic properties), the two SOMOs (singly occupied molecular orbitals), were examined (Figure 6). Interestingly both the SOMOs are not localized on individual copper(II) centers but are delocalized by the participation of largely p-orbitals from oxygen, nitrogen, and carbon atoms of the oxime ligand. This delocalization enhances the extent of antiferromagnetic coupling between the paramagnetic centers, hence leading to the lowering of the open shell singlet state energy with respect to the triplet state. Furthermore, the inspection of SOMOs of complex **2** for the quintet state reveals delocalization in these orbitals (Figure 7). The SOMOs are not confined to individual transition metal centers; rather they engulf the O, C, and N centers of the oximate ligand. Ligand mediated coupling of the paramagnetic transition metal centers may explain the open shell singlet ground state for complex **2** and the weak ferromagnetic coupling in complex **1**.

Oximate bridged dicopper(II) complexes either show strong antiferromagnetic coupling between the magnetic centers for in-plane bonding or show weak ferro- or antiferromagnetic coupling for out-of-plane bonding. For out-of-plane oximate bridged system a quasi-linear correlation between the exchange coupling constant (*J*)

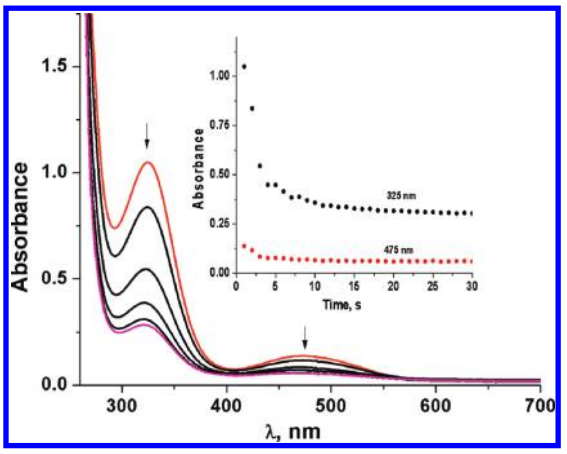

Figure 8. Optical spectral changes during the conversion of **3** (5×10^{-4} M solution in MeCN) to **4** in the presence of 2 equiv of pyridinium perchlorate at room temperature.

Scheme 2. Transformation of **3** to **4** and Vice Versa

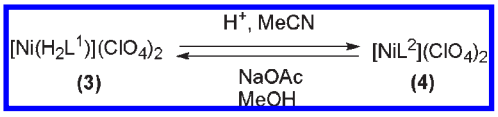

and the Cu−O(oxime)−N(oxime) angle has been proposed.[12] It has been shown from the correlation that a system having this angle less than 106.9° is expected to show ferromagnetic coupling and when this angle is greater than 106.9° the system is expected to show dominant antiferromagnetic coupling. In **1**, this angle is 119.76° and is, therefore, expected to show antiferromagnetic coupling based on the above correlation. But, this is not the case for **1**. This is because of the fact that the coordination geometry of copper(II) center in **1** is distorted trigonal bipyramidal and as a result the oximate oxygen is not an axial donor. The correlation is valid for oximate-bridged complexes having copper(II) centers in square-planar coordination geometry where oximate oxygen is an axial donor. Complex **1** is the first example of a ferromagnetically coupled oximate-bridged complex with trigonal bipyramidal geometry of copper(II) centers and six-membered $M_2(NO)_2$ ring oriented in a boat conformation. A simple magnetostructural correlation warrants more structural data of closely related complexes.

Coupling of Oxime with Nitrile. The crystal structure of **4** indicates that when oxime ligand H_2L^1 reacts with nickel(II) in acetonitrile, the ligand gets iminoacylated and subsequently a mononuclear complex is formed as a result of oxime−nitrile coupling. It is important to note that this coupling does not take place in the absence of nickel(II) ion. The metal templated iminoacylation of oxime is also observed, but slowly, when an acetonitrile solution of complex **3** is kept on stand for about two weeks. In this condition about 30% of the oxime complex is converted to iminoacylated complex **4** followed by the precipitation of dinuclear complex **2**. On the other hand, **4** is not isolated from **2** under similar reaction condition.

Interestingly, the yield of **4** is improved up to 73% (based on the peak at 325 nm) when 2 equiv of pyridinium perchlorate are added to an acetonitrile solution of **3** (Scheme 2). In this condition, the reaction takes about 30 s and the optical spectral changes indicate the decay of

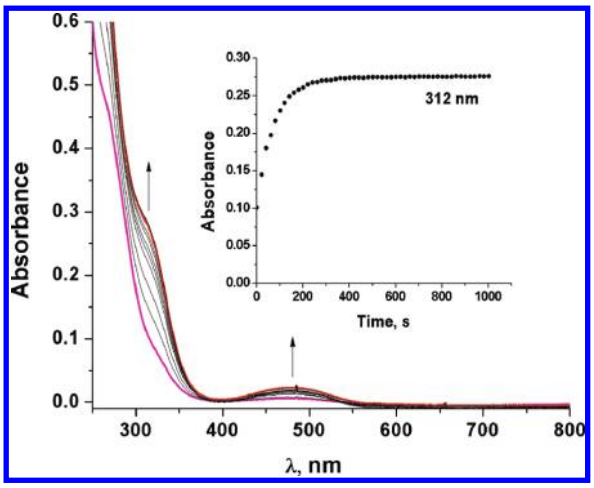

Figure 9. Optical spectral changes during the conversion of **4** (1×10^{-4} M solution in MeOH) to **3** in the presence of 4 equiv of sodium acetate at room temperature.

charge transfer band at 325 nm with time (Figure 8). It is important to mention here that complex **2**, which does not transform to **4** in only acetonitrile, also forms **4** in the presence of pyridinium perchlorate. The results suggest that the coupling reaction possibly occurs via a proton-assisted mechanism.

It has been reported that the iminoacyl derivative of oxime could be transformed to oxime in the presence of sodium acetate.[35] To establish the transformation in this case, a methanolic solution of complex **4** is reacted with sodium acetate and optical spectral changes are monitored with time (Figure 9). It is found that 4 equiv of sodium acetate are needed for maximum conversion of **4** to **3**. A peak for charge transfer transition is generated at 312 nm. Also the d−d band is shifted from 490 to 482 nm, with an increase in absorbance. This establishes the transformation of **3** from **4** with approximately 93% conversion (with respect to the charge transfer band at 312 nm) by hydrolysis of the iminoacyl group with sodium acetate in methanol (Scheme 2).

Inspired by the nickel(II) templated iminoacylation reaction of the oxime groups of H_2L^1 ligand in acetonitrile during the formation of **4**, the reaction was further extended to other nitriles such as butyronitrile and benzonitrile. In both the cases oxime−nitrile coupling were observed.

To investigate the reaction mechanism for the formation of the iminoacyl complex **4**, a computational investigation was conducted. The hybrid DFT study revealed that **4** is the most stable product among all the possible iminoacylated forms. Initially, it was anticipated that the reaction proceeded through nucleophilic attack by the oxime OH group on a metal-bound acetonitrile. Intuitively, one may presume that the metal bound acetronitrile will have an electron deficient carbon vulnerable to nucleophilic attack by the pendant OH group of the oxime; however, it was not possible to locate an intermediate which follows such nucleophilic attack. In fact, the oxime OH showed no propensity to form a bond with the electron deficient carbon of acetonitrile bound to the metal on optimization of initial structural guess which had a bond between the oxime OH and the pertinent carbon. On the contrary when an oximate was considered, it formed a bond to that carbon on optimization of

the initial structural guess. However, the oxime ligand was reluctant to lose a proton to the weakly basic acetonitrile, and it was further confirmed through relevant computations. Hence, the possibility of participation of water molecules and protons in the iminoacylation process was considered. It was found that the oxime

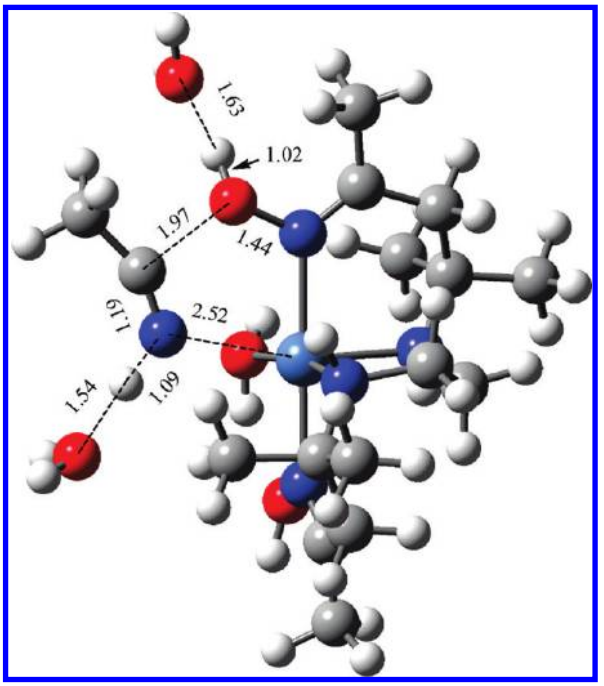

Figure 10. Optimized transition state geometry at the B3LYP level of theory for the formation of the O−C bond in the proton-assisted oxime−nitrile coupling. All bond lengths reported are in angstroms.

nitrogen donors can dissociate at a low barrier of 16 kcal mol^{-1} from the transition metal center and ligand exchange is facile in the reaction mechanism facilitating easy isomerization of the triplet solvated species with axial coordination from solvent (H_2O or MeCN) to an isomeric species with two equatorial solvent molecules, which leads to iminoacylation. The theoretical study revealed that iminoacylation ensues through nucleophilic attack of the oxime OH on a free acetonitrile, whose electrophilicity has been enhanced by a strong hydrogen bond formation to H_3O^+ via its nitrogen donor site (Scheme 3). The relevant transition state is shown in Figure 10. The imaginary mode of this transition state (TS) shows the formation of an O−C bond with concerted proton loss to a water molecule from the oxime OH and a proton gain from the H_3O^+ to the acetonitrile nitrogen. Intrinsic reaction coordinate studies initiated from the TS indeed lead to iminoacylated form as the product and on the reverse trajectory a pentacoordinate nickel(II) complex along with a free acetonitrile hydrogen bonded to H_3O^+ are obtained as reactants. The second iminoacylation proceeds through a similar mechanism. The theoretical findings are in line with the experimental observation of proton dependence of the iminoacylation process. A mechanism has been proposed in Scheme 3 based on the experimental and theoretical results.

Conclusions

The oxime ligand reported in this work forms dimeric copper(II) and nickel(II) complexes with out-of-plane oximate bridging between the metal centers where exchange coupling was found to be different in two complexes. A weak ferromagnetic coupling is operating in the dicopper(II)

Scheme 3. Proposed Mechanism for Oxime−Nitrile Coupling

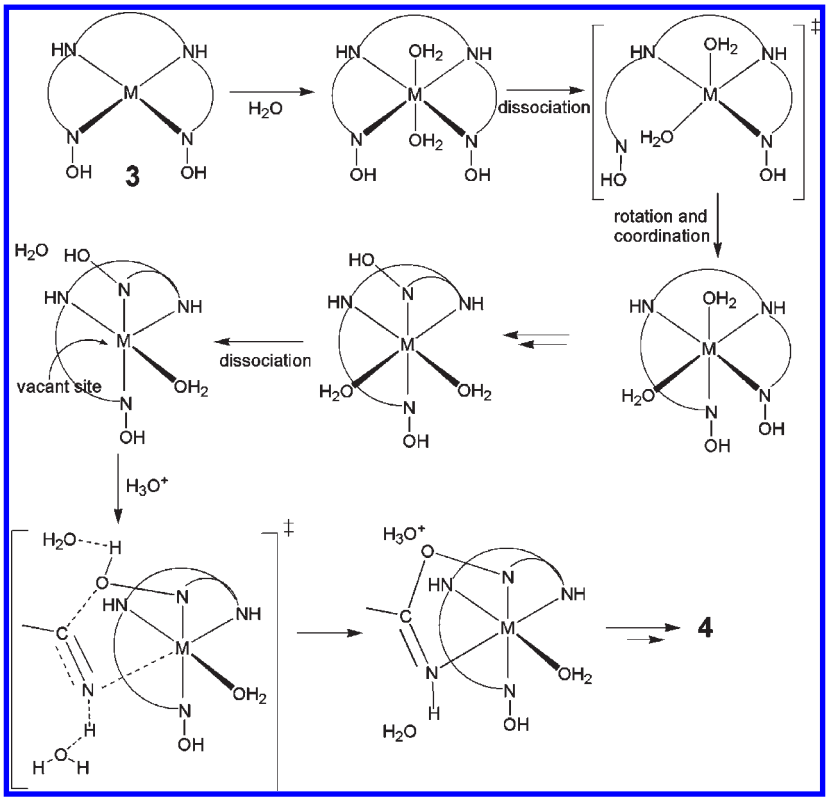

complex while a weak antiferromagnetic coupling is observed in the dinickel(II) complex. The oxime ligand undergoes nickel-mediated coupling with nitriles to form iminoacyl derivatives of oxime. The nickel(II) mediated oxime−nitrile coupling is found to be general for other nitriles. Combined experimental and theoretical results indicate that the nickel-mediated oxime−nitrile coupling takes place via a proton-assisted pathway. The ligand used in this work shows potential in stabilizing different metal complexes with interesting reactivity and magnetic properties.

Acknowledgment. We are grateful to the Department of Science and Technology (DST), Government of India (Project SR/S1/IC-10/2006), for the financial support. Crystal structure determination was performed at the DST-funded National Single Crystal Diffractometer Facility at the Department of Inorganic Chemistry, IACS. All computations were performed at the Aneesur Rahman Centre for High Performance Computing, IACS. The authors acknowledge Mr. Andreas Göbels of Max-Planck-Institut für Bioanorganische Chemie, Mülheim an der Ruhr, Germany, for variable temperature magnetic susceptibility measurements.

Supporting Information Available: Crystallographic data for **1**−**4** in CIF format, optimized geometries in transition states. This material is available free of charge via the Internet at http://pubs.acs.org.